aerospace

MDPI

Article

A Numerical Investigation of Film Cooling under the Effects of Different Adverse Pressure Gradients

Jingwei Shi [1], Zhonghao Hui [1,*], Li Zhou [1,2], Zhanxue Wang [1] and Yongquan Liu [1]

[1] School of Power and Energy, Northwestern Polytechnical University, Xi'an 710072, China; shijw@nwpu.edu.cn (J.S.); zhouli@nwpu.edu.cn (L.Z.); wangzx@nwpu.edu.cn (Z.W.)
[2] Collaborative Innovation Center for Advanced Aero-Engine, Beijing 100191, China
* Correspondence: huizh36@163.com

Abstract: Film cooling needs to be applied to serpentine nozzles due to an increase in thermal load. Adverse pressure gradients (APGs) near the upper wall of such nozzles hinder the forward flow of the coolant, and they may even induce a recirculation zone that complicates the cooling of the film in serpentine nozzles under different APGs. In this study, the film cooling characteristics of a serpentine nozzle under various APGs are investigated through numerical simulations. The studied pressure gradients include strong, moderate, and weak APGs. The results show that the APG weakened the adhesion of the coolant to the surface, thereby reducing the film cooling effectiveness (FCE) and the convective heat transfer coefficient (CHTC). The stronger the APG, the greater its obstructive effect. However, the recirculation zone induced by the strong APG was composed of the coolant, and it adhered tightly to the wall, thereby significantly strengthening the FCE and CHTC. The CHTC under the moderate APG significantly increased due to the convergence of two jets ejected from different holes. For the four blowing ratios, the area-averaged FCE under the strong APG was 29.8% and 24.5% higher than that under the moderate and weak APGs, while the area-averaged ratios of the CHTC under the moderate APG were 1.6% and 16.7% higher than those under the strong and weak APGs. Therefore, more holes should be arranged on the film in the zones of moderate and weak APGs.

Keywords: film cooling; adverse pressure gradient; blowing ratio; flow characteristics; numerical investigation

Citation: Shi, J.; Hui, Z.; Zhou, L.; Wang, Z.; Liu, Y. A Numerical Investigation of Film Cooling under the Effects of Different Adverse Pressure Gradients. *Aerospace* **2024**, *11*, 365. https://doi.org/10.3390/aerospace11050365

Academic Editor: Yang Zhang

Received: 8 April 2024
Revised: 30 April 2024
Accepted: 2 May 2024
Published: 5 May 2024

1. Introduction

The demand for increasingly higher performance has led to an increase in the temperature at the inlet of turbines in the design of modern aero-engines. This, in turn, increases the thermal load on serpentine nozzles and causes problems such as local hot streaks [1,2]. Film cooling technology has good cooling effects and has attracted the attention of many scholars [3,4]. Therefore, film cooling needs to be applied to serpentine nozzles to reduce their temperature and to ensure their viability and appropriate maintenance.

Film cooling technology has been applied to fighter jets, such as F-22 fighter jets and F-35B fighter jets, to reduce the wall temperature and infrared radiation of the exhaust system. Currently, the available research on the film cooling of exhaust systems is mostly focused on high-temperature components, such as conventional nozzle walls and tail cones, which are used to explore film cooling mechanisms and suppress infrared radiation. Matesanz et al. [5] studied the film cooling of a convergent–divergent nozzle by using the k-ε turbulence model. The results showed good agreement between the dimensionless temperature predicted in the numerical simulation and the experimental results under low-Reynolds-number conditions, but the error was larger under high-Reynolds-number conditions. Lebedev et al. [6] experimentally investigated the relationship between film cooling effectiveness and turbulivity in a divergent nozzle. The conclusion showed that an increase in turbulivity significantly reduced the film cooling effectiveness. Straight [7]

explored the film cooling characteristics of an axisymmetric nozzle. They found that shock waves appeared downstream of the cooling groove when the flow inside the nozzle reached supersonic speed, which had a great impact on the film cooling effectiveness. Zheng et al. [8] numerically investigated the effects of film cooling on the plug cone of a two-dimensional vector plug nozzle by using the RNG k-ε turbulence model. The results showed that the wall temperature and infrared radiation could be effectively reduced via film cooling. Zhang et al. [9] analyzed the suppression effect of cooling structures on the infrared radiation of nozzles by using the k-ω SST turbulence model, and they found that the film cooling slot had a better infrared suppression effect than the film cooling holes, but the flow loss of the film cooling slot was greater. Lu et al. [10] conducted an experiment on the film cooling effect of the wall surface and central cone of a binary vectoring nozzle, and they found that the arrangement of the film holes had a great influence on the wall temperature. Wang et al. [11] numerically studied the infrared radiation suppression effect of film cooling in the central cone of an exhaust system by using the SST k-ω model of turbulence. They found that the film cooling of the central cone could effectively suppress the infrared radiation within 0°–15°. Kishik et al. [12] conducted a study on the cooling performance of convergent–divergent nozzles. The experimental results showed that the combination of film cooling and impingement cooling could effectively reduce the temperature of the nozzle wall. Hui et al. [13,14] numerically studied the effects of the structural parameters of cooling holes on the film cooling of a serpentine nozzle by using the k-ω SST turbulence model. They found that, as the inclination angle increased, the area-averaged FCE first increased and then decreased. However, they did not focus on the effects of different adverse pressure gradients, and the film cooling characteristics were not comprehensively studied. Currently, conventional nozzles are the main research objects for examining the film cooling of exhaust systems, and most studies adopt the RANS method for numerical calculations. The flow characteristics of conventional nozzles are relatively simple. However, the flow field structure of serpentine nozzles is complex; the flow inside the curved channel presents typical non-uniform characteristics.

Complex pressure gradients appear in serpentine nozzles that bring different film cooling effects from other structures [15,16]. Abdelmotalib et al. [17], Shan et al. [18], and He et al. [19] studied the mechanism of flow through a serpentine nozzle. The results showed that there were transverse pressure gradients, as well as complex vortex structures. Sun et al. [20–23] further found that a region of local acceleration and an adverse pressure gradient (APG) were induced due to the large curvature, and the serpentine nozzle exhibited typical non-uniform characteristics. Sun et al. [24,25] investigated serpentine nozzles' flow field using numerical and experimental methods, and they concluded that the APG appeared near the upper wall, the bent structure of which could lead to hot streaks. Crowe et al. [26,27] studied serpentine nozzles' flow mechanism, and they claimed that variations in their cross-section and curvature led to a streamwise vortex that could induce a hot streak on their walls. In summary, a curved pipeline leads to complex pressure gradients and strong swirls, which pose daunting challenges to the design of film cooling for serpentine nozzles.

As the most prominent characteristic of flow in a serpentine nozzle, the APG significantly influences the characteristics of film cooling. The mainstream pressure gradient's effect on the film cooling has been extensively investigated. Lutum et al. [28] concluded that an APG had limited effects on film cooling effectiveness (FCE), while a strong FPG had a significant influence on FCE. Coletti et al. [29] found that the mainstream pressure gradient had a squeezing impact on the film and enhanced the strength of a kidney-shaped vortex. Jessen et al. [30] studied the structure of the flow field under the influence of the mainstream APG by using the PIV technique. The experimental results showed that the APG had a significant impact on the thickness of the boundary layer and the depth of penetration of the coolant into the mainstream. Konopka et al. [31] drew a similar conclusion to that in Ref. [30]. They also found that the mainstream APG had few effects on FCE. Qin et al. [32] found that the mainstream pressure gradient had a minor effect on FCE at a

high blowing ratio. Wang et al. [33] numerically investigated the impact of the mainstream pressure gradient on FCE. Their results showed that the mainstream pressure gradient influenced mixing between the mainstream and the coolant, the thickness of the boundary layer, and the strength of the vortex. In summary, the APG influences the interaction between the mainstream and the coolant, thereby yielding complex outcomes. Moreover, some of the above conclusions regarding the effects of the pressure gradient on film cooling are contradictory. This attests to the complex influence of APGs when they are coupled with many other factors.

In summary, studies examining the APG focus on flat plates and curved surfaces. The results show that the APG influences the mixing characteristics of the coolant and may lead to complex film cooling performances. Meanwhile, the influence of the APG is coupled with many factors, such as the wall curvature and the mainstream's velocity. There are strong, moderate, and weak adverse pressure gradients inside a serpentine nozzle, as well as a swirl and a complex distribution of vortices. Therefore, the film cooling characteristics near the APG region of a serpentine nozzle are complex. The aim of this study is to clarify the influence of these different APGs in order to establish a reliable method for the film cooling of serpentine nozzles. In this study, we examine a serpentine nozzle's film cooling characteristics under strong, moderate, and weak APGs using numerical simulations. The characteristics of film cooling include those of flow, as well as the distributions of FCE and the convective heat transfer coefficient (CHTC).

2. Geometric Model and Numerical Method

2.1. Geometric Model

The geometric model is shown in Figure 1. Detailed procedures for the design of serpentine nozzles have been provided in Ref. [34]. The stealth performance and aerodynamic characteristics of serpentine nozzles should be comprehensively considered during the process of structural design. The shape of a serpentine nozzle's cross-section gradually changes from circular to rectangular. The area of the cross-sections gradually decreases from the front to the back, and the area ratio between the outlet and the inlet is 0.448. The major design parameters of the serpentine nozzle and their values are shown in Table 1. Three rows of holes are implemented in a serpentine nozzle to succinctly represent this structure. The acceleration factor has been widely used to measure the magnitude of the pressure gradient [30–33]. It is defined as $K = (\nu/u^2) \times (\mathrm{d}u/\mathrm{d}x)$, where ν is the coefficient of dynamic viscosity, and u is the velocity of the mainstream. A negative value represents the APG, while a positive value represents the FPG. The smaller the acceleration factor, the stronger the APG. As shown in Figure 1c, the intensity of the APG changed from strong to weak, and the zone of the APG was located between X/L = 0.36 and X/L = 0.50. We set 19 film cooling holes in the zones of strong, moderate, and weak APGs, which were located at X/L = 0.37, X/L = 0.41, and X/L = 0.45, respectively. The hole diameter (D) was 2 mm, the hole injection angle (α) was 35°, and the spacing between holes (G) was 6 mm.

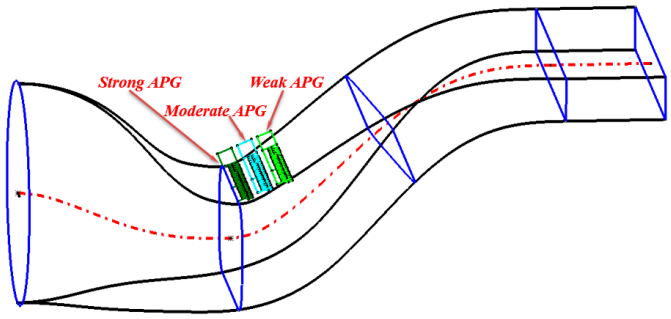

(**a**)

Figure 1. *Cont.*

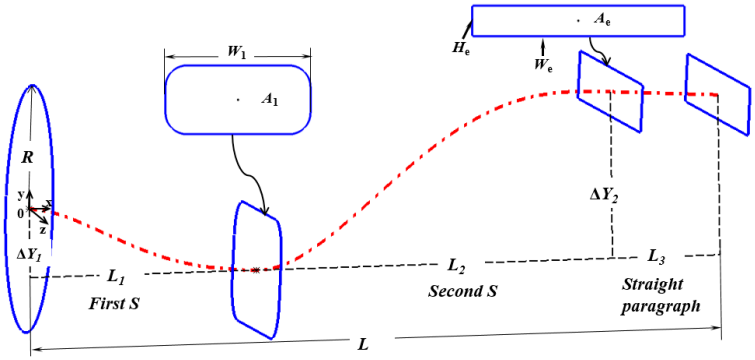

(**b**)

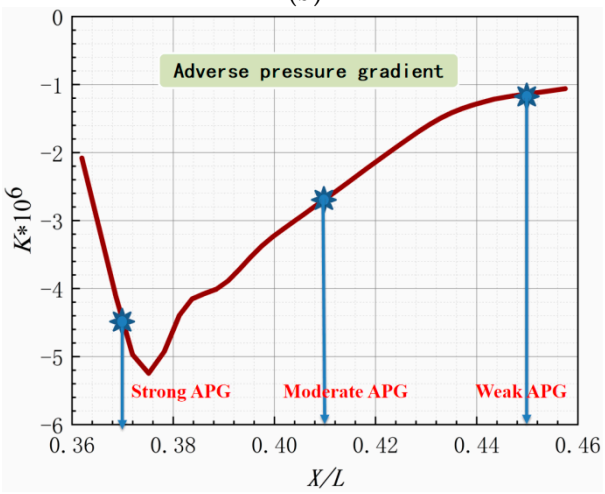

(**c**)

Figure 1. Proposed geometric model. (**a**) Serpentine nozzle subjected to film cooling. (**b**) Geometric parameters of serpentine nozzle. (**c**) Acceleration factor distributions on serpentine nozzle's upper wall.

Table 1. Major design parameters and their values.

Parameter	Value
Contraction ratio of first serpentine paragraph A_1/A_{in}	0.61
Offset distance of first serpentine centerline $\triangle Y_1$ (mm)	52.5
Exit aspect ratio W_e/H_e	6
Offset distance of second serpentine centerline $\triangle Y_2$ (mm)	159.8
Total length of nozzle L (mm)	505.19
Ratio of length of first S passage to that of second L_1/L_2	0.67

2.2. Validation Study

An experiment was conducted in a test facility with a dual-flow exhaust system to further validate the numerical method. The experimental platform is shown in Figure 2a, and it involved the use of pressure-sensitive paint (PSP). This facility was equipped with a mainstream system, a secondary flow system, a system to measure the flow field, and a measurement system for the PSP. The boundary conditions used for the validation were as follows: the pressure ratio of the nozzle was 1.5, and the blowing ratio was 0.4. Figure 2b shows a comparison between the FCE predicted by the proposed model and that obtained from the experimental data. It shows that the *k*-ω SST model of turbulence yielded a highly accurate laterally averaged FCE of the serpentine nozzle. There was little variation between the experimental data and the numerical results calculated by the model, and their profiles exhibited identical trends. Therefore, the proposed numerical method is reliable.

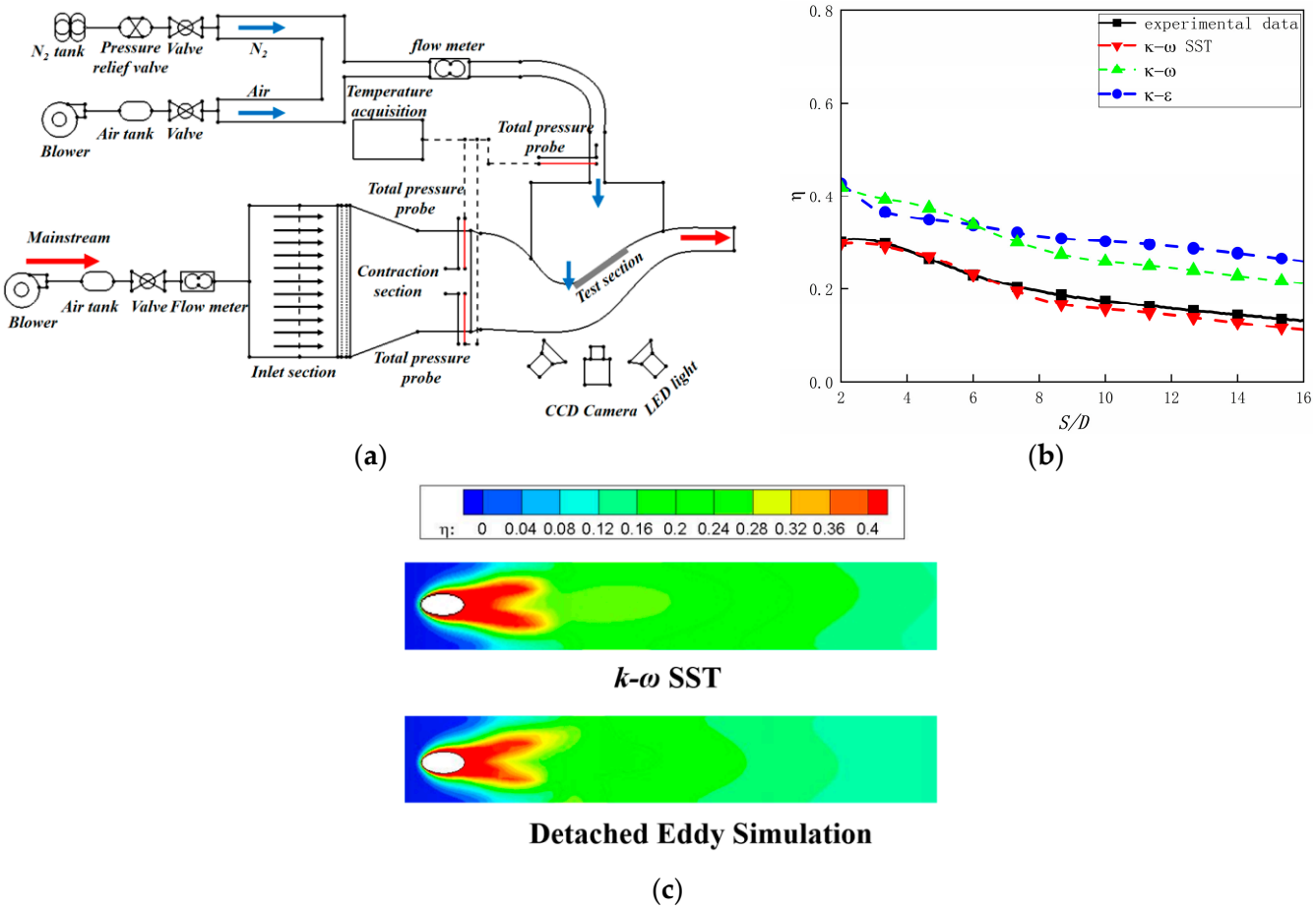

Figure 2. Validation of geometric model. (**a**) Experimental facility. (**b**) Comparison of laterally averaged FCE. (**c**) Comparison of FCE contours.

In order to explore more advanced numerical methods, the Detached Eddy Simulation (DES) is applied in this study. The original geometric model described in Section 2.1 is scaled down by 10 times, and the number of grids used by the DES is 25 million. In order to ensure sufficient time accuracy, the time step is set to 6×10^{-6} s. The average courant number is 0.94, which meets the requirements of the DES calculation. The coolant's mass flow rate needs to be recalculated, and the settings of other boundary conditions are the same as those in the steady state. In the unsteady calculation, monitoring points are set at the outlet of the serpentine nozzle to monitor changes in local physical quantities. When the fluctuation of the physical quantity of the monitoring point shows a very regular change and the calculation residual is stable below 10^{-6}, the calculation is convergent. Figure 2c shows the film cooling effectiveness contours on the serpentine nozzle wall, including the RANS results and DES results. The distribution of the film cooling characteristics calculated by the RANS and DES is similar. Limited by the computing capacity, the SST *k-ω* model of turbulence is chosen for the following study.

2.3. Numerical Method

Simulations were processed in ANSYS CFX software (version 18.0) using the finite element method, and structured grids were created in ICEM software. The structured computational grids of the model of calculation are shown in Figure 3a. Three-dimensional (3D) numerical calculations were conducted. The grid was set with y+ < 5, and it was designed to grow exponentially layer by layer away from the wall for 30 layers to ensure the valid growth of the boundary layer. Grid independence was verified by using three sets of structures with 20 million (N_1), 35 million (N_2), and 50 million grids (N_3), and the values of the laterally averaged FCE obtained by using them are compared in Figure 3b.

The results show that the values of the laterally averaged FCE for N_2 and N_3 were close to each other. However, the maximum error between N_1 and N_2 was 19%. Therefore, N_2 was chosen for the subsequent simulations. The compressible, steady, Reynolds-averaged N–S equations were solved. The SST k-ω model of turbulence was applied.

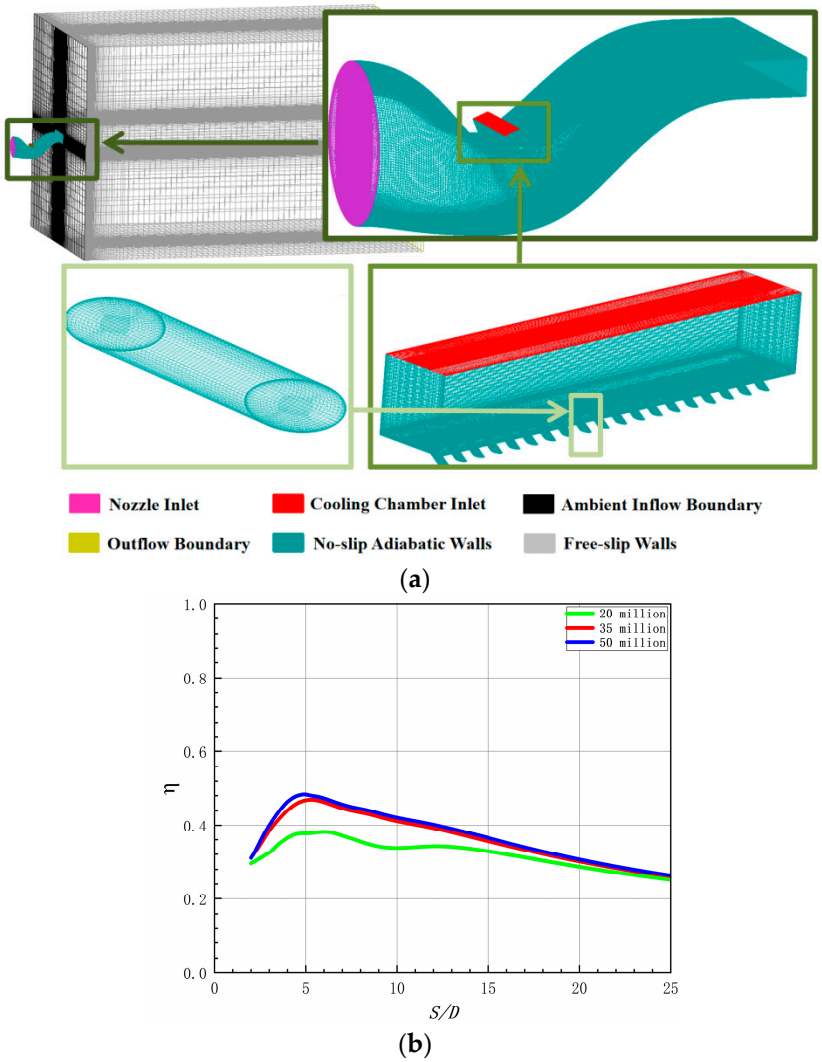

Figure 3. Numerical method. (**a**) Computational grid and numerical boundary conditions. (**b**) Verification of grid independence.

The boundary conditions are shown in Figure 3a, and their values are shown in Table 2. The pressure inlet conditions were used for the nozzle inlet. The mass flow rate conditions were used for the inlet of the cooling chamber, and the coolant's mass flow is related to the blowing ratio. The definition of the blowing ratio is presented in Section 2.4. The blowing ratios used in this study included 0.3, 0.6, 0.9, and 1.2, and the flow parameters at the strong, moderate, and weak APGs are shown in Table 3. The conditions for the outlet of pressure were applied to the boundary of outflow, while the far-field conditions of pressure were applied to the boundary of ambient inflow. Non-slip adiabatic boundary conditions were set for the boundaries of the solid wall.

Table 2. The values of boundary conditions.

Parameter	Value
Nozzle inlet total pressure P_1* (Pa)	222,915
Nozzle inlet total temperature T_1* (K)	1734
Coolant total temperature T_c* (K)	482
Nozzle exit environment back pressure P_b (Pa)	101,325
Ambient freestream static pressure P_0 (Pa)	101,325
Ambient freestream static temperature T_0 (K)	300

Table 3. Flow parameters at the strong, moderate, and weak APGs.

Parameter	Strong APG	Moderate APG	Weak APG
Coolant mass flow rate at M = 0.3 (kg/s)	0.00367	0.00326	0.00309
Coolant mass flow rate at M = 0.6 (kg/s)	0.00734	0.00652	0.00618
Coolant mass flow rate at M = 0.9 (kg/s)	0.01101	0.00978	0.00927
Coolant mass flow rate at M = 1.2 (kg/s)	0.01468	0.01304	0.01236
Mainstream local velocity u_{local} (m/s)	632	502	458

2.4. Definition of Parameters

The film cooling effectiveness η and the convective heat transfer coefficient h are applied to evaluate the film cooling characteristics.

The film cooling effectiveness is expressed as

$$\eta = \frac{T_r - T_{aw}}{T_r - T_c} \tag{1}$$

where T_{aw} is the temperature of the adiabatic wall, T_c is the temperature of the coolant, and T_r is the recovery temperature.

The convective heat transfer coefficient is expressed as

$$h = \frac{q}{T_w - T_{aw}} \tag{2}$$

where T_w is the wall temperature in the case of film cooling, and T_{aw} is the wall adiabatic temperature in the case of film cooling. Liu et al. [35] claimed that the heat flow rate of the wall (q) does not influence the magnitude or distribution of the CHTC. We set the heat flow rate of the wall to 300,000 W/m^2 in this study.

The ratio of the convective heat transfer coefficient (CHTC), h/h_0, was used to describe the characteristics of heat transfer. The CHTC ratio h/h_0 is the ratio of the CHTC in the presence of film cooling to that without it under the same working conditions of the mainstream.

The nozzle pressure ratio (NPR) is expressed as

$$NPR = \frac{P_1^*}{P_0} \tag{3}$$

where P_1^* is the total pressure of the nozzle inlet, and P_0 is the ambient pressure.

The blowing ratio (M) is expressed as

$$M = \frac{\rho_c u_c}{\rho_\infty u_\infty} \tag{4}$$

where ρ_c is the coolant's density, u_c is the coolant's velocity, ρ_∞ is the mainstream's density, and u_∞ is the mainstream's velocity.

3. Results and Discussion

3.1. Flow Characteristics

As shown in Figure 4, the structures of flow in the holes under different APGs were similar to one another. Due to the inclination of the holes, separation occurred inside them on the side of the sharp angle of their inlet when the coolant flowed from the cooling chamber into the holes, and a low-speed zone formed. The compressed airflow accelerated into the holes in the film from the side of the blunt angle at their inlet. As the zone of low-speed flow subsequently shrank, it gradually expanded and flowed toward the outlet of the holes in the film to form an "air column" after being sprayed out, and it had an obstructive effect on the mainstream. The coolant simultaneously bent toward the wall and adhered to it under the action of the mainstream, and this changed the temperature of the mainstream near the wall, as well as the heat transfer between the mainstream and the wall.

Figure 4 shows that the APG mainly influenced the structure of flow downstream of the holes. The APG hindered the downstream flow of the coolant, and it was not conducive to the attachment of the coolant to the wall. The stronger the APG, the more prominent the above phenomenon, and it might have even caused the coolant to flow back near the wall. When the blowing ratio was 0.3, the strong APG had the strongest obstructive effect on the coolant, and a large amount of the coolant near the wall broke away from its main body and flowed in the opposite direction to form a recirculation zone. The coolant outside this recirculation zone was squeezed by other airflow and thus occupied a small space. The obstructive effect of the moderate APG was weak such that most of the coolant flowed downstream, but a recirculation zone was still induced, and it was 60% smaller than that induced by the strong APG. The coolant outside the recirculation zone occupied a larger space, and its speed decreased significantly along the direction perpendicular to the wall. The weak APG could not induce a recirculation zone, and all the coolant flowed downstream in the same direction. The weak APG caused the coolant to decelerate, and the low-speed region formed by it was 70% smaller than that formed by the strong APG.

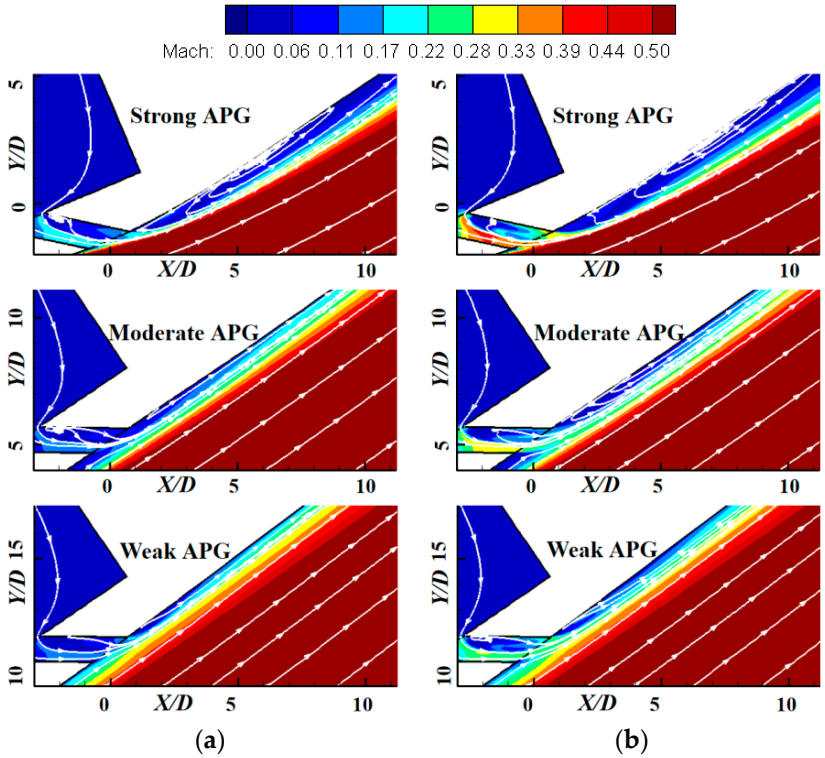

Figure 4. *Cont.*

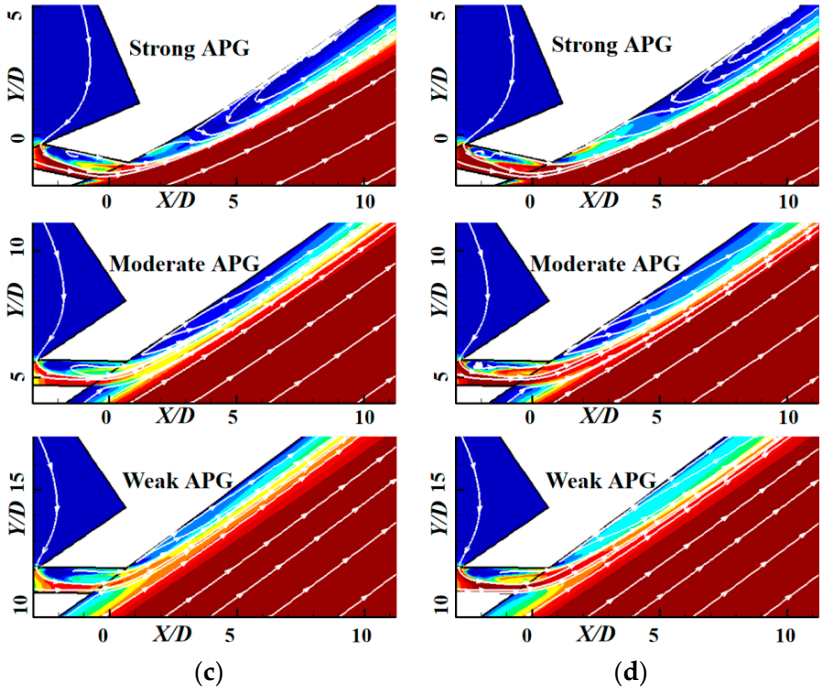

Figure 4. The contours of Ma and the distributions of the streamlines. (**a**) M = 0.3; (**b**) M = 0.6; (**c**) M = 0.9; (**d**) M = 1.2.

Remarkably, the squeezing effects of the mainstream flow on the coolant were also different under the three APGs. From front to back, the pressure gradient first changed from an FPG to a strong APG, then to a moderate APG, and finally to a weak APG. The mainstream flow near the zone of the strong APG was first accelerated by the FPG, such that the mainstream velocity was high, and the thickness of the wall layer in front of the holes was the smallest. Meanwhile, the strong adverse pressure gradient zone was located on the convex wall, and its curvature was large. Therefore, the squeezing effect of the mainstream on the coolant was the strongest. Remarkably, for the same blowing ratio, the coolant's mass flow rate of the strong APG was the largest, which enhanced the squeezing effect of the mainstream. The mainstream flow close to the moderate APG first underwent deceleration owing to the strong APG, such that the mainstream velocity was low, and the thickness of the wall layer was the largest. Meanwhile, the curvature of the convex surface decreased along the flow direction, and the coolant's mass flow rate decreased. Therefore, the squeezing effect of the mainstream on the coolant was the worst. The mainstream velocity near the weak APG was higher than that near the moderate APG, and the effect of the extrusion of the mainstream on the coolant was stronger than that near the moderate APG.

When the blowing ratio was 0.6, more coolant flowed near the wall such that the recirculation zones of the strong and moderate APGs expanded, as did the low-speed region of the weak APG. The region of the recirculation zone caused by the moderate APG was 60% smaller than that caused by the strong APG, and the low-speed region caused by the weak APG was 60% smaller than that caused by the strong APG. When the blowing ratio was 0.9, the speed of the coolant was relatively high, and it could resist obstruction by the APG. The recirculation zone induced by the strong APG moved downstream, while the moderate APG could not induce a recirculation zone, but the low-speed region formed by it continued to expand. At this time, the region of recirculation caused by the moderate APG was 40% smaller than that caused by the strong APG. However, the weak APG had a smaller obstructive effect on the coolant, and its low-speed region shrank. For M = 1.2, the recirculation zone caused by the strong APG continued to move downstream. The low-speed region continued to shrink in the case of the moderate and weak APGs.

There are complex vortex structures in serpentine nozzles, such as oppositely rotating vortices near the corner of cross-sections, which have an effect on film cooling. Figure 5 shows the distribution of vorticity on cross-sections downstream of the holes in the film at S/D = 0, S/D = 6, S/D = 12, and S/D = 18. The S is the curvature coordinate, whose origin is the center of the film hole's outlet. It shows a counter-rotating vortex pair (CRVP) in the core region of the jet sprayed from the holes in the film. This feature was discovered by Goldstein et al. [36] in a study on film cooling. Leylek [37] analyzed the mechanism of film cooling and concluded that the vortices formed by the distribution of velocity of the boundary layer inside the holes and the shear effect of the jet sprayed out of the holes in the film on the mainstream were the main causes of the formation of the CRVP in the core region downstream of the holes in the film, with the former factor playing a dominant role. The CRVP had two negative effects: one was that its aerodynamic effect vertically lifted the coolant such that it deviated from the wall to reduce its coverage, and the other was that it caused the hot mainstream flow to move to the wall, thereby reducing the cooling effect of the coolant. The CRVP could not occupy the entire coolant and instead mainly occupied the region outside the recirculation zone. Figure 5 shows that, when the coolant flowed through the recirculation zone formed by the strong APG, the CRVP gradually detached from the wall. It induced an anti-counter-rotating vortex pair (ACRVP) in the recirculation zone. This ACRVP caused the jet to adhere to the wall and the coolant to move laterally, which was the opposite to the effect of the CRVP. The moderate APG also induced a recirculation zone at low blowing ratios, but the recirculation zone's region was too small in this case to promote the development of an ACRVP such that the CRVP occupied the entire region. The weak APG did not lead to a recirculation zone under any blowing ratio such that an ACRVP did not develop.

In summary, the APG hindered the flow of the coolant. The stronger the APG, the greater its obstructive effect. The squeezing effects of the mainstream on the coolant also influenced the flow characteristics, and this was related to the upstream pressure gradients, the wall layer thickness in front of the cooling holes, the wall curvature, and the centripetal accelerations. The strong APG led to the formation of a recirculation zone under various working conditions, while the moderate APG led to its formation only at low blowing ratios. The weak APG did not induce any recirculation zone and only caused the coolant to decelerate. The fully developed recirculation zone caused by the strong APG promoted the development of an ACRVP, while the underdeveloped recirculation zone did not. ACRVPs did not develop in the cases of the moderate and weak APGs.

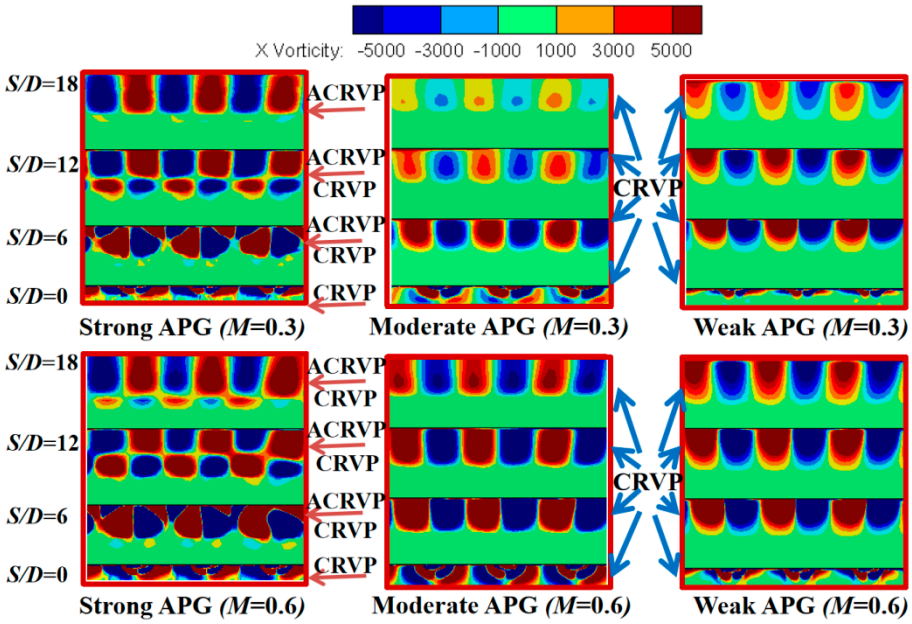

Figure 5. *Cont.*

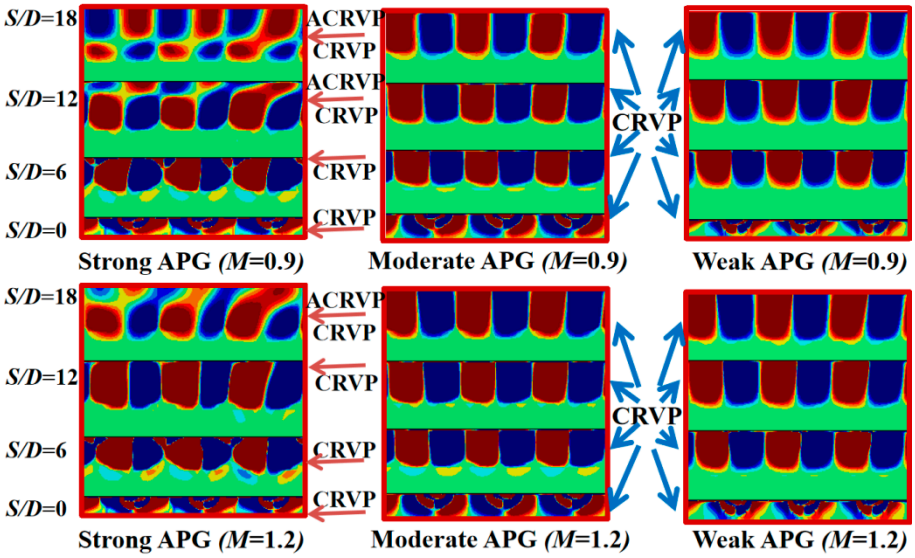

Figure 5. The distributions of vorticity on cross-sections downstream of the film holes.

3.2. Characteristics of Distribution of Film Cooling Effectiveness

Figure 6 shows the contours of the FCE. According to the above analysis, the recirculation zone induced by the strong APG promoted the development of an ACRVP, which mainly influenced the distribution of the FCE owing to the strong APG. The moderate and weak APGs did not induce a sufficiently strong obstructive effect to induce a fully developed recirculation zone, such that the distributions of their FCE were mainly determined by the CRVP.

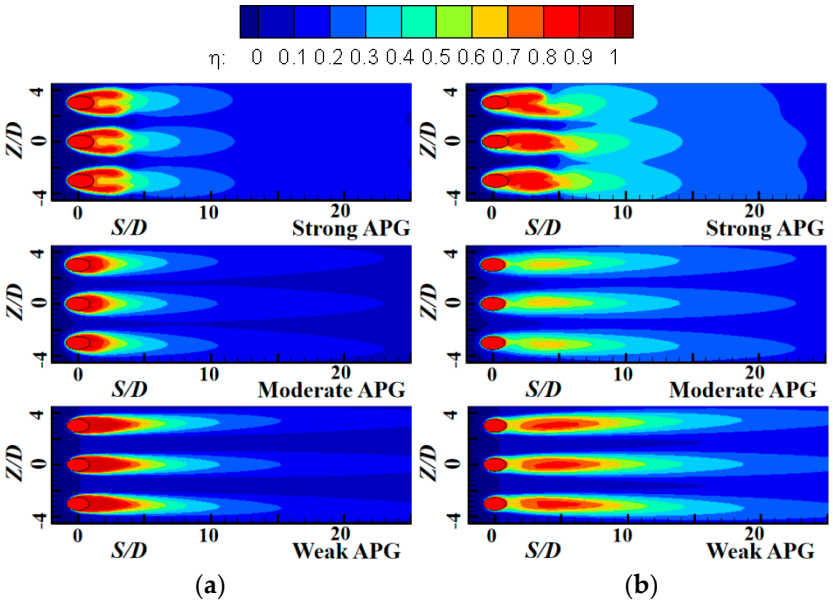

Figure 6. *Cont.*

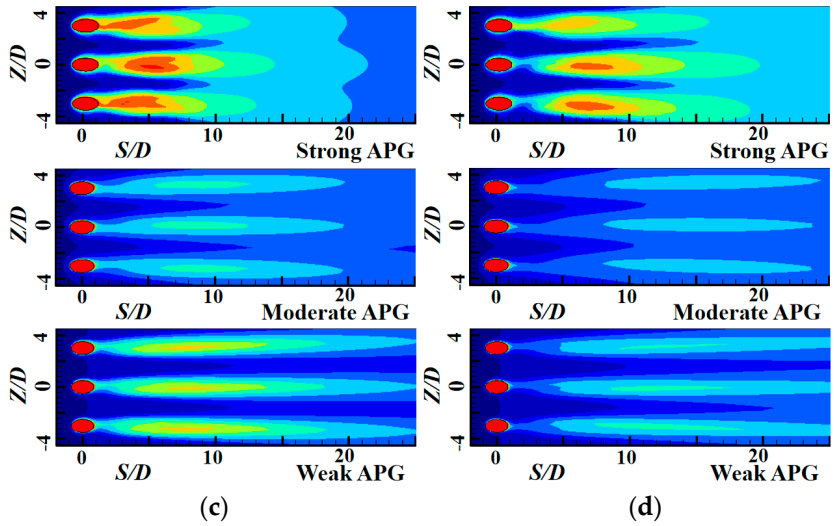

Figure 6. Contours of film cooling effectiveness. (**a**) M = 0.3; (**b**) M = 0.6; (**c**) M = 0.9; (**c**) M = 1.2.

When the blowing ratio was 0.3, the mass flow rate of the coolant was low, it adhered well to the wall and had a large area of coverage near the outlet of the holes in the film along the direction of flow and that lateral to it, and the coverage of the coolant was sound at $S/D < 5$. Differences were observed in the distributions of the FCE under the different APGs. Under the strong APG, the FCE near the centerline of the hole in the film was low, while that on both sides away from the centerline was higher. This was due to the effect of the ACRVP, which brought the coolant from the central area to the edge of the surface of the wall. The recirculation zone induced by the strong APG was squeezed not only by the mainstream but also by the coolant outside the recirculation zone. Meanwhile, the mainstream's squeezing effect was intensified by the large wall layer thickness and the large curvature of the convex surface. Therefore, the adhesion and ductility of the coolant were the highest, and the coolant in the recirculation zone covered the widest range along the lateral direction. It also had good coverage along the direction of flow. Under the moderate APG, the FCE in the central area was slightly higher than that along the edge. This was caused by the CRVP, and the weak APG exhibited a similar distribution of the FCE. The coolant under the moderate APG still covered a wider range along the lateral direction, but the recirculation zone was not fully developed, and the effect of the squeezing of the mainstream was the weakest, such that the FCE of the moderate APG was the lowest of the three APGs. The region with a high FCE of the moderate APG was 50% smaller than that of the strong APG. Under the weak APG, the coolant covered a smaller region along the lateral direction and a larger region along the direction of flow. Although there was no recirculation zone, the coolant was subjected to a stronger squeezing effect from the mainstream and weaker obstruction from the APG, such that the FCE of the weak APG was higher than that of the moderate APG but lower than that of the strong APG. As cold air flowed downstream, it continuously mixed with the mainstream, and the trajectory of the jet significantly weakened.

When the blowing ratio was 0.6, the mass flow rate of the coolant increased, and some of it began to break away from the control of the mainstream boundary layer. The coolant separated from the surface of the wall, and this caused the width of its lateral coverage near the outlet of the hole to decrease to about two-thirds of that at M = 0.3. However, due to the increase in the mass flow of the coolant, the length of its coverage along the direction of flow increased to about twice that at M = 0.3. Under the strong APG, the recirculation zone and large mainstream's squeezing effect strengthened the coolant's adhesion and yielded the highest FCE. Under the moderate and weak APGs, the FCE near the outlet of the holes decreased, while that downstream of the holes in the film increased. Of the three APGs, the coolant's lateral coverage under the strong APG was the widest, while its coverage along the direction of flow under the weak APG was the longest. The lateral

coverage of the coolant under the moderate APG was also relatively wide, but its overall FCE was lower than that under the strong and weak APGs. As the blowing ratio was further increased, a larger volume of the coolant broke away from the surface, and the jet trajectory significantly weakened. The recirculation zone under the strong APG still yielded a better cooling effect. When the blowing ratio was increased to 1.2, the improvement in the FCE due to the recirculation zone became more prominent, and the cooling effect of the strong APG was much higher than that of the moderate and weak APGs.

The laterally averaged distributions of the FCE are shown in Figure 7a–d. When the blowing ratio was 0.3, the volume of the coolant gradually decreased as it flowed downstream, such that the laterally averaged FCE decreased along the direction of flow under all three types of APGs. Remarkably, the laterally averaged FCE under the strong APG fluctuated around $S/D = 5$. The recirculation zone enhanced the coolant's adhesion and ductility under the strong APG, such that it could cover the widest range along the lateral direction and a longer range along the direction of flow. The laterally averaged FCE of the strong APG was the highest. Under the moderate APG, the coolant encountered resistance from the APG, and the squeezing effect of the mainstream was the weakest, because of which the coolant had poor adhesion and ductility. Meanwhile, the recirculation zone under the moderate APG was not fully developed, because of which it was not sufficient to improve the effect of film cooling. Therefore, the FCE of the moderate APG was the lowest of the three APGs. Although no recirculation zone formed under the weak APG, the squeezing effect of the mainstream was large, and the coolant encountered weaker obstruction from the APG such that the FCE was higher than that under the moderate APG but lower than that under the strong APG. At $M = 0.3$, the momentum of the coolant was low, and it could adequately cover the wall after it flowed out of the hole. The influence of the APG was thus minor, and the values of the laterally averaged FCE of the different APGs were similar to one another. When the blowing ratio was 0.6, part of the coolant first escaped from the wall and then attached to it again, because of which the laterally averaged FCE first increased and then decreased. The laterally averaged FCE under the strong APG fluctuated around $S/D = 5$, and this phenomenon was also observed at $M = 0.3$. Compared with the results at $M = 0.3$, the laterally averaged FCE of the strong APG at $M = 0.6$ was higher than that of the moderate and weak APGs. Therefore, the recirculation zone induced by the APG played a more important role in improving the FCE at higher blowing ratios. When the blowing ratio was 0.9, the recirculation zone moved downstream, as did the ACRVP, and the fluctuations near the hole in the film induced by the recirculation zone disappeared. The laterally averaged FCE of the strong APG was much larger than that of the moderate and weak APGs, especially near the outlet of the holes in the film, while the laterally averaged FCE of the moderate APG was similar to that of the weak APG. The distributions of the laterally averaged FCE at $M = 1.2$ were similar to those at $M = 0.9$, the recirculation zone induced by the strong APG significantly improved the laterally averaged FCE, and the value of the latter was 50% higher than that of the moderate and weak APGs.

The distributions of the area-averaged FCE are shown in Figure 7e. The area ranged from $S/D = 2$ to $S/D = 25$. As the blowing ratio was increased under the strong APG, a larger volume of the coolant attached to the wall due to the recirculation zone, and the area-averaged FCE increased. As the blowing ratio was increased under the moderate and weak APGs, the area-averaged FCE first increased and then decreased. When the blowing ratio was low, the volume of the coolant was too low to cover a sufficient area of the surface, but it was adequate to cover the region near the hole at the outlet of the film. As the blowing ratio was increased further, the coolant covered a greater length, but its adhesiveness worsened. The strong APG exhibited an advantage in terms of improving the area-averaged FCE, which contributed to the recirculation zone. As the blowing ratio was increased, the advantage of the strong APG became more significant. When considering all four blowing ratios, we found that the area-averaged FCE under the strong APG was 29.8% and 24.5% higher than that under the moderate and weak APGs.

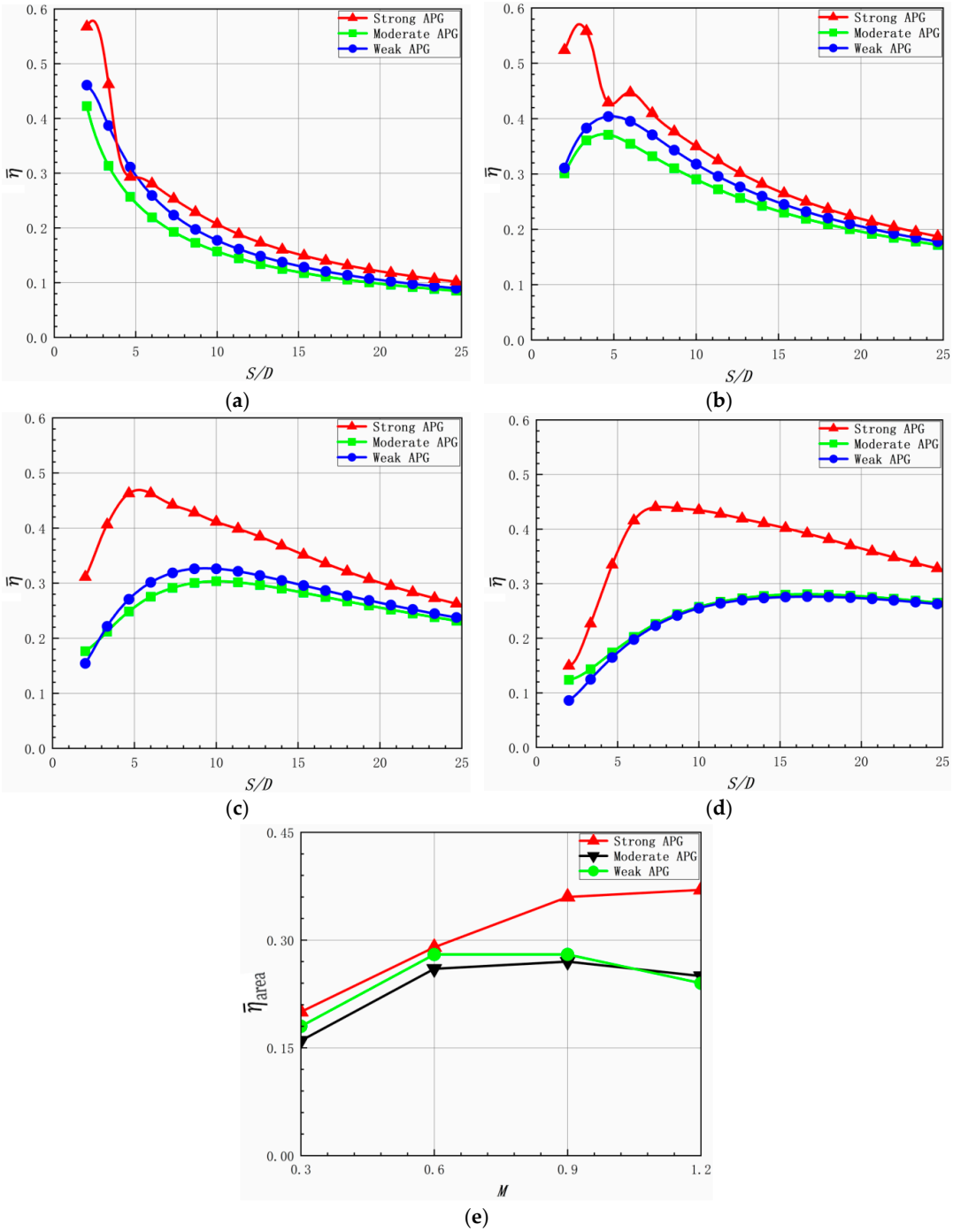

Figure 7. Distributions of film cooling effectiveness. (**a**) Laterally averaged FCE at M = 0.3. (**b**) Laterally averaged FCE at M = 0.6. (**c**) Laterally averaged FCE at M = 0.9. (**d**) Laterally averaged FCE at M = 1.2. (**e**) Area-averaged FCE.

3.3. Distribution of Convective Heat Transfer Coefficient

Figure 8 shows the contours of the CHTC ratio. When the blowing ratio was 0.3, the coolant was squeezed and quickly adhered to the wall under the strong APG. Meanwhile, the large wall layer thickness in front of the holes and the large curvature of the convex surface strengthened the squeezing effect of the mainstream on the coolant. This strengthened convective heat transfer between the coolant and the wall and led to a high CHTC ratio near the exit of the holes in the film. An ACRVP developed quickly in the recirculation zone. However, the ACRVP was squeezed by the CRVP, and the two vortices that constituted the

ACRVP moved to the boundary of the adjacent holes. The space between the adjacent holes was small and caused the ACRVP to split and reorganize into the CRVP near the boundary. The CRVP impinged on the edge behind the boundary, thereby reducing the thickness of the boundary layer of the region of impingement and significantly enhancing the intensity of convective heat transfer. Therefore, the CHTC ratio of the edge was higher than that of the central region. As the coolant flowed downstream, the trajectory formed by the CRVP gradually weakened. The recirculation zone was small under the moderate APG, the ACRVP was not fully developed, and the CRVP still occupied the core of the coolant. The CRVP split and reorganized into an ACRVP near the boundary. This ACRVP impinged on the central position behind the boundary. Therefore, the CHTC ratio at the central position was higher than that at the edge. No recirculation zone formed for the weak APG. The coolant encountered low resistance, such that most of it flowed downstream and covered a smaller region along the lateral direction. Therefore, the intensity of the convergence of the two jets ejected from different holes weakened, and the intensity of the CRVP was low. Although the distributions of the CHTC ratio caused by the weak APG were similar to those caused by the moderate APG, the CHTC ratio itself was lower. In summary, the CHTC ratio was the highest under the strong APG, followed by the moderate APG, and it was the lowest under the weak APG.

When the blowing ratio was 0.6, more coolant flowed close to the wall, and the CHTC ratio increased. The jets in adjacent holes collided and converged near the boundary of the holes in the film. This enhanced convective heat transfer, and the CHTC under the moderate APG increased drastically. The CHTC ratio under the moderate APG was the highest near the outlet of the holes, but the CHTC ratio of the strong APG was the highest in the back region. The distribution of the CHTC ratio under M = 0.9 and M = 1.2 was similar to that under M = 0.6. Remarkably, as the coolant flowed downstream under the strong APG, the CRVP in the boundary split and reorganized into an ACRVP behind the holes. Therefore, the distribution of the CHTC ratio under the strong APG changed. The CHTC ratios of the three APGs increased with the blowing ratio.

The distributions of the laterally averaged CHTC ratio are shown in Figure 9a–d. When the blowing ratio was 0.3, the laterally averaged CHTC ratio first decreased and then increased until it became stable under the strong APG. The CRVP gradually detached from the wall along the direction of flow near the exit of the holes in the film, because of which the laterally averaged CHTC ratio decreased along the direction of flow. As the coolant continued to flow downstream, the ACRVP became the main factor influencing the ratio of convective heat transfer. The ACRVP closely adhered to the wall. Therefore, the ratio of the laterally averaged CHTC increased gradually. This is because the ACRVP was present in the recirculation zone, and it exchanged a large amount of heat with it. Therefore, the laterally averaged CHTC ratio of the strong APG was the highest. The CRVP influenced the distribution of the CHTC ratio under the moderate and weak APGs. The coolant adhered to the wall near the exit of the hole in the film. When the coolant flowed downstream, its volume decreased such that the laterally averaged CHTC ratio also decreased. The squeezing effect of the mainstream was the weakest under the moderate APG, and the recirculation zone had not fully developed, such that heat exchange between the coolant and the surface of the wall was low. However, the jets of the adjacent holes collided and converged near the boundary of the holes in the film, which enhanced convective heat transfer. Therefore, the ratio of the laterally averaged CHTC of the moderate APG was higher than that of the weak APG but lower than that of the strong APG. No recirculation zone formed under the weak APG, and there was no strong intersection between the jets of adjacent holes. The ratio of the laterally averaged CHTC of the moderate APG was thus the lowest of the three APGs. When the blowing ratio was 0.6, more coolant flowed close to the wall, and the CHTC ratio increased. The ratio of the laterally averaged CHTC first decreased and then increased before stabilizing under the strong APG, while it decreased under the moderate and weak APGs. The strong intersection between the jets of adjacent holes under the moderate APG enhanced the CHTC near the outlet of the holes, because of

which the ratio of the CHTC of the moderate APG was the highest. However, the CHTC ratio of the strong APG was the highest for $S/D > 8$ due to the recirculation zone. When the blowing ratio was 0.9 under the strong APG, the CRVP in the boundary split and reorganized into an ACRVP behind the holes as the coolant flowed downstream. This caused the CHTC ratio to first decrease and then increase along the direction of flow. The location of the intersection of the jets moved downstream under the moderate APG, because of which the CHTC ratio first increased and then decreased along the direction of flow. The CHTC ratio of the moderate APG was the highest for $S/D < 13$. The distribution of the ratio of the laterally averaged CHTC at $M = 1.2$ was similar to that at $M = 0.9$. The intersection of the jets of adjacent holes under the moderate APG significantly improved the ratio of the laterally averaged CHTC, which was 15% higher than that under the strong and weak APGs.

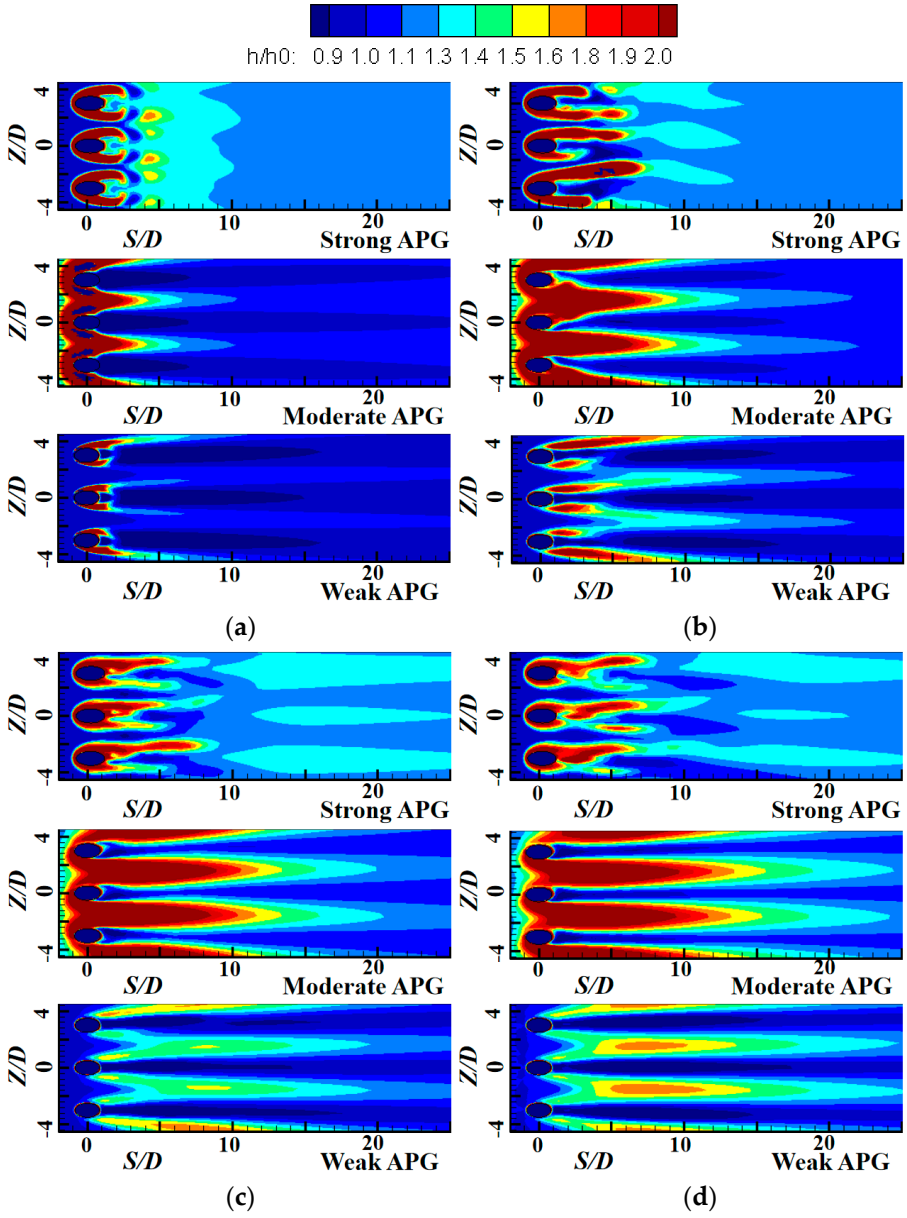

Figure 8. Contours of the ratio of the convective heat transfer coefficient. (**a**) $M = 0.3$. (**b**) $M = 0.6$. (**c**) $M = 0.9$. (**d**) $M = 1.2$.

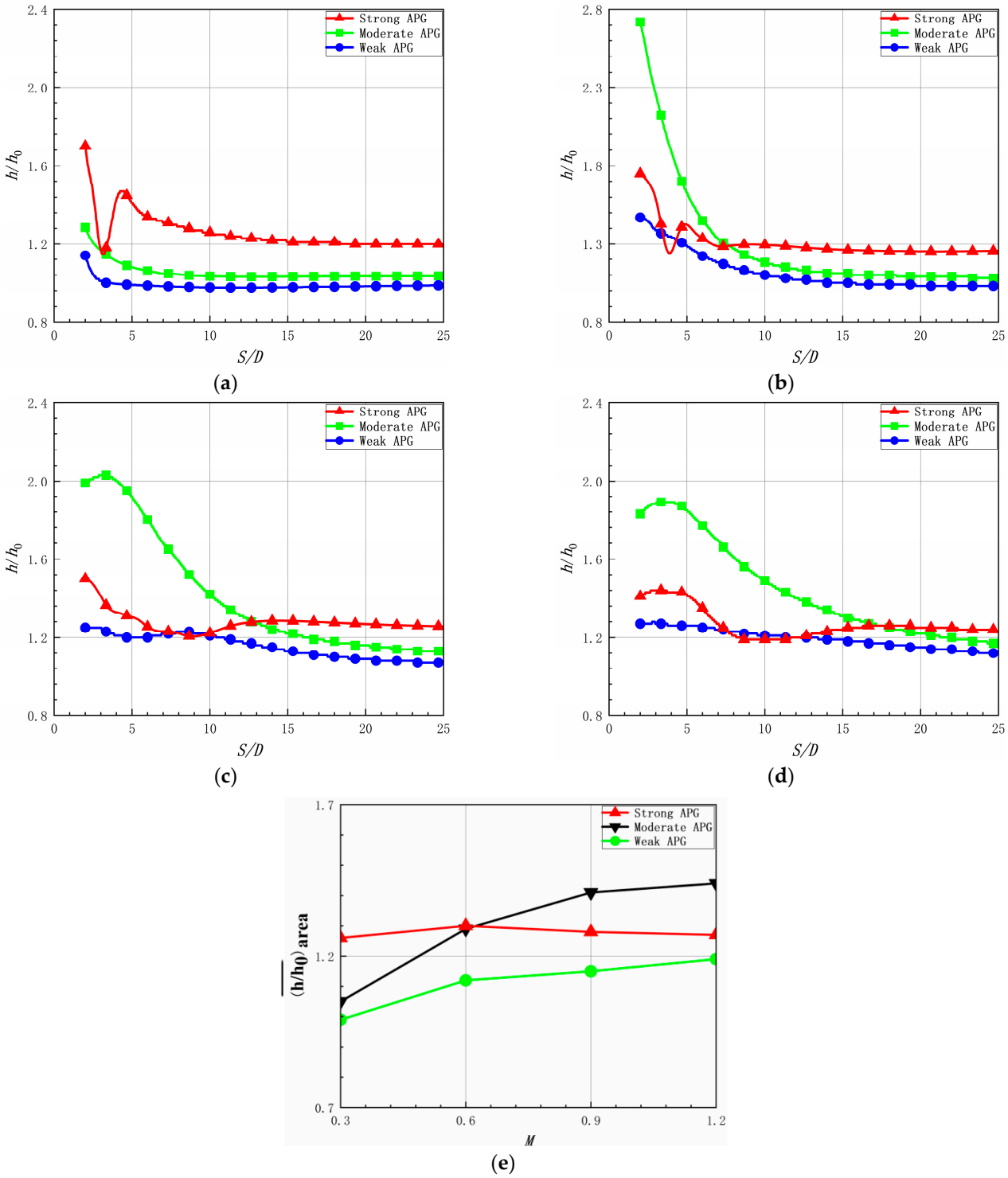

Figure 9. Distributions of ratio of laterally averaged convective heat transfer coefficient. (**a**) Ratio of laterally averaged CHTC at M = 0.3. (**b**) Ratio of laterally averaged CHTC at M = 0.6. (**c**) Ratio of laterally averaged CHTC at M = 0.9. (**d**) Ratio of laterally averaged CHTC at M = 1.2. (**e**) Ratio of area-averaged CHTC.

The distributions of the area-averaged CHTC ratio are shown in Figure 9e. As the blowing ratio increased under the strong APG, the area-averaged CHTC ratio first increased and then decreased. The recirculation zone formed by the strong APG enhanced the CHTC, and the values of the area-averaged CHTC ratio under the different blowing ratios were similar to one another. As the blowing ratio increased under the moderate and weak APGs,

the momentum of the coolant increased, as did the CHTC ratio. The above analysis shows that the recirculation zone caused by the strong APG enhanced the CHTC under all blowing ratios, especially at low blowing ratios. The convergence of two jets under the moderate APG also enhanced the CHTC, especially at high blowing ratios. Therefore, the ratio of the area-averaged CHTC under the strong APG was the highest at $M = 0.3$ and $M = 0.6$, while that of the moderate APG was the highest at $M = 0.9$ and $M = 1.2$. When considering all four blowing ratios, we found that the ratios of the area-averaged CHTCs under the moderate APG were 1.6% and 16.7% higher than those under the strong and weak APGs.

4. Conclusions

The aim of this study was to clarify the influence of different adverse pressure gradients (APGs) in order to establish a reliable method for the film cooling of serpentine nozzles. In this study, the film cooling characteristics of a serpentine nozzle under weak, moderate, and strong APGs were investigated numerically. The film cooling characteristics included the flow characteristics, as well as the distributions of the film cooling effectiveness (FCE) and convective heat transfer coefficient (CHTC). The main conclusions are as follows:

The flow characteristics downstream of the film holes were greatly influenced by the APGs and the mainstream's squeezing effect. The APG hindered the flow of the coolant. The stronger the APG, the greater its obstructive effect. A strong obstructive effect will induce a recirculation zone, but a large kinetic energy of the coolant will have the opposite effect. Therefore, the strong APG led to the formation of a recirculation zone under various working conditions, the moderate APG led to the formation of a recirculation zone only at a low blowing ratio, and the weak APG only caused the coolant to decelerate. Affected by the wall layer thickness in front of the cooling holes, the wall curvature, the centripetal accelerations, and the upstream pressure gradients, the squeezing effect of the mainstream flow on the coolant under the strong APG was the largest, followed by that under the weak APG, while the effect of the squeezing of the coolant under the moderate APG was the smallest.

The FCE was mainly influenced by the recirculation zone and the extrusion of the mainstream. The recirculation zone induced by the strong APG was mainly composed of the coolant, and it was subjected to the strongest squeezing effect from the mainstream. Therefore, the coolant in the recirculation zone was able to adequately cover the surface of the wall, thereby yielding the highest FCE. The moderate APG still posed a strong obstruction to the coolant but could not induce a recirculation zone. Meanwhile, the squeezing effect of the mainstream was the weakest, because of which the FCE under the moderate APG was the lowest. The weak APG offered the weakest hindrance to the flow of the coolant. The coolant was thus able to cover a wider range along the direction of flow. The squeezing effect of the mainstream was strong in this case, because of which the FCE under the weak APG was higher than that under the moderate APG. As the blowing ratio was increased, the advantage of the strong APG in terms of improving the FCE became more prominent due to the recirculation zone. When considering all four blowing ratios, we found that the area-averaged FCE under the strong APG was 29.8% and 24.5% higher than that under the moderate and weak APGs.

The CHTC distributions were mainly influenced by the recirculation zone and the convergence of two jets ejected from different holes. The recirculation zone induced by the strong APG adhered to the wall, which enhanced convective heat transfer between the coolant and the wall, especially at low blowing ratios. The convergence of two jets under the moderate APG also enhanced the CHTC. The distribution of the CHTC under the weak APG was similar to that under the moderate APG. However, the coverage of the coolant along the lateral direction was poor, as was the convergence of two jets ejected from different holes, and the CHTC was thus lower. As the blowing ratio was increased, the area-averaged CHTC ratios of the strong APG remained unchanged, but the CHTC ratios of the moderate and weak APG increased significantly because of the convergence of two jets, and the moderate APG showed great advantages in improving the CHTC. When

considering all four blowing ratios, we found that the ratio of the area-averaged CHTCs under the moderate APG were 1.6% and 16.7% higher than those under the strong and weak APGs.

Author Contributions: Conceptualization, J.S. and Z.H.; Methodology, J.S., Z.H., L.Z. and Z.W.; Software, J.S. and Z.H.; Validation, J.S.; Formal Analysis, J.S. and Z.H.; Resources, L.Z., Z.W. and Y.L.; Writing—Original Draft Preparation, J.S. and Z.H.; Writing—Review and Editing, J.S. and Z.H.; Project Administration, L.Z., Z.W. and Y.L. All authors have read and agreed to the published version of the manuscript.

Funding: This research was funded by the Fundamental Research Funds for the Central Universities and Science Center for Gas Turbine Project (P2022-B-II-010-001, P2022-B-I-002-001); the National Natural Science Foundation of China (52376032, 52076180); Funds for Distinguished Young Scholars of Shaanxi Province (2021JC-10); and National Science and Technology Major Project (J2019-II-0015-0036).

Data Availability Statement: Data will be made available on request.

Conflicts of Interest: The authors declare that they have no known competing financial interests or personal relationships that could have appeared to influence the work reported in this paper.

Nomenclature

Parameter name		
h	convective heat transfer coefficient	$W/m^2 \cdot K$
K	acceleration factor	
M	blowing ratio	
P	pressure (unit: Pa)	Pa
q	heat flow rate (unit: $W \cdot m^{-2}$)	
S	curvature coordinate	
T	temperature	K
X	streamwise coordinate	
Y	spanwise coordinate	
Z	vertical coordinate	
Greek alphabet		
α	film cooling hole injection angle	°
η	adiabatic film cooling efficiency	
Abbreviations		
ACRVP	anti-counter-rotating vortex pair	
APG	adverse pressure gradient	
CHTC	convective heat transfer coefficient	
CRVP	counter-rotating vortex pair	
FCE	film cooling effectiveness	

References

1. Crowe, D.S.; Martin, C.L. Hot streak characterization of high-performance double serpentine exhaust nozzles at design conditions. *J. Propuls. Power* **2019**, *35*, 501–511. [CrossRef]
2. Yang, X.; Zhang, K.; Yao, J.X.; Wu, J.M.; Lei, J.; Xiong, Y.; Wang, H. Experimental and numerical investigations of vane endwall film cooling with different cooling hole configurations. *Aerosp. Sci. Technol.* **2023**, *142*, 108658. [CrossRef]
3. Duan, X.L.; Chang, J.L.; Chen, G.S.; Liu, T.S.; Ma, H. Contribution of different parameters on film cooling efficiency based on the improved orthogonal experiment method. *Aerospace* **2024**, *11*, 67. [CrossRef]
4. Shen, Z.; Hu, B.M.; Li, G.Z.; Zhang, H.J. Large eddy simulation of pulsed film cooling with a dielectric barrier discharge plasma actuator. *Aerospace* **2024**, *11*, 28. [CrossRef]
5. Matesanz, A.; Veldzquez, A.; Rodriguez, M. Performance of algebraic and k-ε models in the study of film cooling problems inside convergent-divergent nozzles. In Proceedings of the 30th AIAA/ASME/SAE/ASEE Joint Propulsion Conference, Indianapolis, IN, USA, 27–29 June 1994.
6. Lebedev, V.P.; Lemanov, V.V.; Terekhov, V.I. Film-cooling efficiency in a laval nozzle under conditions of high freestream turbulence. *J. Heat Transf.* **2006**, *128*, 571–579. [CrossRef]
7. Straight, D.M. Effect of shocks on film cooling of a full scale turbojet exhaust nozzle having an external expansion surface. In Proceedings of the 15th AIAA/SAE/ASME Joint Propulsion Conference, Las Vegas, NV, USA, 18–20 June 1979.

8. Zheng, J.S.; Shan, Y.; Zhang, J.Z. Cooling and infrared radiation suppression effect of plug trailing-body of two-dimensional vector plug nozzle. *Acta Aeronaut. Et Astronaut. Sin.* **2017**, *38*, 121384.
9. Zhang, B.; Ji, H.H.; Zhang, Z.B.; Luo, M.D. Numerical investigation of effect of truncated cone with different cooling structures on infrared suppressing characteristics of nozzle cavities. *J. Aerosp. Power* **2014**, *29*, 2362–2367.
10. Lu, H.H.; Ji, H.H.; Wang, D.; Liu, J.; Wang, H. Experimental on infrared characteristics suppression by component cooling of two-dimensional convergent-divergent vectoring nozzle exhaust system. *J. Aerosp. Power* **2017**, *32*, 2070–2079.
11. Wang, X.; Zhang, J.Z.; Shan, Y. Effects of film hole arrangement on central-cone cooling and infrared radiation characteristics of exhaust system. *J. Aerosp. Power* **2016**, *31*, 830–835.
12. Kishi, K.; Joubert, H. Research of 2-D Variable Exhaust Nozzle. *Int. J. Gas Turbine Propuls. Power Syst.* **2019**, *5*, 17–22. [CrossRef] [PubMed]
13. Hui, Z.H.; Shi, J.W.; Zhou, L.; Jiao, L.Y.; Wang, R.; Wang, Z.X.; Liu, Y.Q. The influence of the adverse pressure gradient on the flow characteristics of a serpentine nozzle with film cooling. *Aerosp. Sci. Technol.* **2023**, *136*, 108256. [CrossRef]
14. Hui, Z.H.; Shi, J.W.; Zhou, L.; Wei, X.Z.; Sun, X.L. Effect of inclination angle on the film cooling in a serpentine nozzle with strong adverse pressure gradient. *Phys. Fluids* **2023**, *35*, 1–15.
15. Zhang, L.H.; Qian, B.; Zhang, C.R.; Mao, J.; Fan, H.R. Numerical study on the cooling characteristics of cat-ear-shaped film-cooling holes on turbine blades. *Case Stud. Therm. Eng.* **2022**, *36*, 1–12. [CrossRef]
16. Prapamonthon, P.; Yin, B.; Yang, G.W.; Zhang, M.H. Understanding of temperature and cooling effectivenesss sensitivity of a film-cooled vane under coolant inlet temperature effect: A case study. *Case Stud. Thermal Eng.* **2019**, *14*, 1–10. [CrossRef]
17. Abdelmotalib, H.M.; Lee, C.; Seo, Y.; Lee, J. A computational study of two-dimensional serpentine nozzle performance with different annular mixer configurations. *Int. J. Mech. Sci.* **2021**, *208*, 106690. [CrossRef]
18. Shan, Y.; Zhou, X.M.; Tan, X.M.; Zhang, J.Z.; Wu, Y.H. Parametric design method and performance analysis of double S-shaped nozzles. *Int. J. Aerosp. Eng.* **2019**, *2019*, 1–24. [CrossRef]
19. He, Y.B.; Yang, Q.Z.; Gao, X. Comprehensive optimization design of aerodynamic and electromagnetic scattering characteristics of serpentine nozzle. *Chin. J. Aeronaut.* **2021**, *34*, 118–128. [CrossRef]
20. Sun, X.L.; Wang, Z.X.; Zhou, L.; Shi, J.W.; Liu, Z.W. Experimental and computational investigation of double serpentine nozzle, Proceedings of the Institution of Mechanical Engineers. *Part G J. Aerosp. Eng.* **2015**, *229*, 2035–2050.
21. Sun, X.L.; Wang, Z.X.; Zhou, L.; Shi, J.W.; Cheng, W. Flow characteristics of double serpentine convergent nozzle with different inlet configuration. *ASME J. Eng. Gas Turbines Power* **2018**, *140*, 1–12.
22. Sun, X.L.; Wang, Z.X.; Zhou, L.; Liu, Z.W.; Shi, J.W. Influences of design parameters on a double serpentine convergent nozzle. *J. Eng. Gas Turbines Power* **2016**, *138*, 700–710. [CrossRef]
23. Sun, X.L.; Wang, Z.X.; Zhou, L.; Shi, J.W.; Cheng, W. Internal flow and external jet characteristics of double serpentine nozzle with different aspect ratio, Proceedings of the Institution of Mechanical Engineers. *Part G J. Aerosp. Eng.* **2019**, *233*, 545–560.
24. Sun, P.; Zhou, L.; Wang, Z.X.; Shi, J.W. Temperature distributions of internal flow and external jet fields of double serpentine convergent nozzle for turbofan. *Xibei Gongye Daxue Xuebao/J. Northwestern Polytech. Univ.* **2021**, *39*, 1331–1339. [CrossRef]
25. Sun, P.; Zhou, L.; Wang, Z.X.; Shi, J.W. Influences of geometric parameters on serpentine nozzles for turbofan. *Aerosp. Sci. Technol.* **2013**, *136*, 108224. [CrossRef]
26. Crowe, D.S.; Martin, C.L. Effect of geometry on exit temperature from serpentine exhaust nozzles. In Proceedings of the 53rd AIAA Aerospace Sciences Meeting, Kissimmee, FL, USA, 5–9 January 2015.
27. Crowe, D.S.; Martin, C.L. Hot streak characterization in serpentine exhaust nozzles. In Proceedings of the 52nd AIAA/SAE/ASEE Joint Propulsion Conference, Salt Lake City, UT, USA, 25–27 July 2016.
28. Lutum, E.; Wolfersdorf, J.; Semmler, K. An experimental investigation of film cooling on a convex surface subjected to favorable pressure gradient flow. *Int. J. Heat Mass Transf.* **2001**, *44*, 939–951. [CrossRef]
29. Coletti, F.; Elkins, C.J.; Eaton, J.K. An inclined jet in crossflow under the effect of streamwise pressure gradient. *Exp. Fluids* **2013**, *54*, 1–16. [CrossRef]
30. Jessen, W.; Konopka, M.; Schroeder, W. Particle image velocimetry measurements of film cooling in an adverse pressure gradient flow. *J. Turbomach.* **2012**, *134*, 1–13. [CrossRef]
31. Konopka, M.; Jessen, W.; Meinke, M. Large-eddy simulation of film cooling in an adverse pressure gradient flow. *J. Turbomach.* **2013**, *135*, 1–16. [CrossRef]
32. Qin, Y.M.; Chen, P.T.; Ren, J.; Jiang, H.D. Effects of wall curvature and streamwise pressure gradient on film cooling effectiveness. *Appl. Therm. Eng.* **2016**, *107*, 776–784. [CrossRef]
33. Wang, W.Q.; Shan, Y.; Liao, H.L. Numerical research on film cooling effectiveness with different mainstream pressure gradient. *J. Aerosp. Power* **2017**, *32*, 1876–1885.
34. Hui, Z.H.; Shi, J.W.; Zhou, L.; Wang, Z.X.; Liu, Y.Q. Experimental investigation of serpentine nozzles for turbofan. *Aerosp. Sci. Technol.* **2021**, *117*, 106892. [CrossRef]
35. Liu, C.L.; Gao, C.; Wolfersdorf, J.V. Numerical study on the temporal variations and physics of heat transfer coefficient on a flat plate with unsteady thermal boundary conditions. *Int. J. Therm. Sci.* **2017**, *113*, 20–37. [CrossRef]

36. Eckert, E.R.G.; Goldstein, R.J.; Ramsey, J.W. Film cooling with injection through holes: Adiabatic wall temperature downstream of a circular hole. *J. Eng. Power.* **1968**, *90*, 384–393.
37. Walters, D.K.; Leylek, J.H. A detailed analysis of film-cooling physics: Part 1: Streamwise injection with cylindrical holes. *J. Turbomach.* **2000**, *122*, 102–112. [CrossRef]